QUARKONIA*

By S. Ono

CERN — Geneva**

(Received September 1, 1983)

Various properties (spectra, decays, mixings, etc.) of quarkonium states are studied systematically by using potential models, quark pair creation models, and unitarized quarkonium models.

PACS numbers: 14.80.Dq

1. Introduction

Since the discovery [1] of the J/ψ in November 1974, many authors [2–6] have studied the potential between the quark and the antiquark. We have learned that the potential is Coulombic near the origin, as can easily be understood from QCD, and that it has a confining part for large distances. A similar (Coulombic part plus confining part) potential for quarks in baryons (or potential between quark and diquark) had already been proposed [7] in 1973 from the phenomenological analysis of elastic ep and electroproduction processes.

Potential models turned out to be very successful for quarkonium states. From the recent discovery [8] of the $\Upsilon(1P)$ state by the CESR group, we learned that the potential quarkonium model is still the only model which explains the heavy quarkonium up to now.

Although the motion of a quark inside light hadrons is relativistic, the Schrödinger theory is surprisingly successful, even for them. Isgur and Karl [9] and others [10] have shown that the baryon spectra can be nicely described by the Schrödinger theory with the harmonic oscillator potential.

By using a single potential, meson and baryon spectra are studied simultaneously and systematically by Schöberl and myself [11]. Success of this model (especially for P states) is impressive, and this model helps us to understand the nature of some controversial mesons, e.g., $\iota(1440)$, $\theta(1640)$, $g_T(2160)$ etc.

* Presented at the XXIII Cracow School of Theoretical Physics, Zakopane, May 29 — June 12, 1983.

** Address: CERN TH, 1211 Genève 23, Switzerland.

The potential model is also powerful for predicting various decay rates of quarkonium states. The quark pair creation model (QPC) [12–14] allows us to describe the OZI allowed decay rates above threshold. The QPC has been first checked [14–16] by the study of strong decays of light mesons. It is found [13, 16, 17] by using the QPC and other models that the decay properties of ϱ' and radially excited $c\bar{c}$ are strongly influenced by the node structure of wave functions.

Recent data [8] by the CESR group on $\Upsilon''' \to B\bar{B}$ are consistent with the QPC predictions [18, 19]. Υ''' is found [8] to be 32 MeV above $B\bar{B}$ threshold. This is already too high (see Section 3.2 of this paper) to use the simple phase space formula $\Gamma \propto k^{2l+1}$.

Below the threshold decay processes of quarkonium states are mainly classified [20] into three types:

(*i*) annihilation; the decay rates are proportional to the wave function at the origin (or the derivative);

(*ii*) transitions;

(*iii*) spontaneous decays of Q and $\bar{Q}$ inside $Q\bar{Q}$, leaving another particle as a spectator.

Since we have fairly good knowledge of quarkonium states, we can reliably predict [20] spectra and decay rates of toponium states. Of course, we cannot exclude the possibility that the decay properties of toponium states might be unexpectedly disturbed by the production of particles predicted by certain theories such as SUSY.

Charmonium states, for example, strongly couple to the $D\bar{D}$, $D\bar{D}^*$, etc., channels which give large widths above threshold. Because of unitarity and analyticity, these channels also contribute large mass shifts both below and above threshold. By combining the unitarized quarkonium model (UQM) [21] and QPC, one finds [22] negative mass shifts of order 100 MeV for $c\bar{c}$ states and smaller mass shifts for $b\bar{b}$ states. Decay rates of S and D charmonium states $\to e^+ + e^-$ can only be understood by including such unitarity effects [22].

2. A potential model for quarkonium states [11]

2.1. A quarkonium potential

We start from a typical QCD-motivated quarkonium potential [11] which is of the Coulomb type at short distance and linear for large R.

$$V(R) = V_1(R) - be^{-R/c} + V_0,$$

$$V_1(R) = \begin{cases} -\dfrac{4\alpha_s}{3R} + d & \text{for} \quad R < R_1; \\ aR & \text{for} \quad R \geqslant R_1. \end{cases} \tag{2.1}$$

We show that almost all well-established quarkonium mass levels (from $u\bar{u} \pm d\bar{d}$ to $b\bar{b}$, from 1S to radially and orbitary excited states) can be reproduced by using this potential (completely flavour-independent potential).

2.2. Breit-Fermi Hamiltonian

The one-gluon exchange gives rise to a Breit-Fermi Hamiltonian:

$$H_{LS} = A\vec{L}\cdot\vec{S}+D\vec{L}\cdot\vec{S}^{-}, \quad H_T = B(3\vec{\sigma}_1\cdot\hat{R}\vec{\sigma}_2\cdot\hat{R}-\vec{\sigma}_1\cdot\vec{\sigma}_2), \quad H_{SS} = C\vec{\sigma}_1\cdot\vec{\sigma}_2,$$

$$A = \frac{1}{R}\frac{d}{dR}\left[\left\{\frac{1}{m_1m_2}+\tfrac{1}{4}\left(\frac{1}{m_1^2}+\frac{1}{m_2^2}\right)\right\}V_v-\tfrac{1}{4}\left(\frac{1}{m_1^2}+\frac{1}{m_2^2}\right)V_v\right],$$

$$D = \tfrac{1}{4}\left(\frac{1}{m_1^2}-\frac{1}{m_2^2}\right)\frac{1}{R}\left(\frac{dV_v}{dR}-\frac{dV_s}{dR}\right),$$

$$B = -\frac{1}{12m_1m_2}\left(\frac{d^2}{dR^2}-\frac{1}{R}\frac{d}{dR}\right)V_v,$$

$$C = \frac{1}{6m_1m_2}\Delta V_v, \quad \vec{S} = \vec{S}_1+\vec{S}_2, \quad \vec{S}^{-} = \vec{S}_1-\vec{S}_2, \tag{2.2}$$

where V_v is the fourth component of the vector potential and V_s is the scalar part of the potential. This is the non-relativistic reduction of the Bethe-Salpeter equation. We assume

$$V_s = aR,$$

$$V_v = V(R)-aR. \tag{2.3}$$

2.3. Spin-spin force with a finite range

A typical way of calculating the spin-dependent force is to compute Eq. (2.2) perturbatively. This method is problematic, since H_{SS} is too large to treat perturbatively. There are three methods for avoiding this difficulty.

(*i*) Calculate the mass matrix of H_{SS} by using unperturbed wave functions of 1S, 2S, 1D, ... states and diagonalize it [see, for example, Ref. [23]].

(*ii*) Include the H_{SS} in the potential. Smear H_{SS} by a suitable function if it is too singular.

(*iii*) Choose the potential whose singularity is soft enough and include H_{SS} in the potential [see, for example, Ref. [24]].

We use the second method. Since H_{SS} contains a negative constant $\times\,\delta(\vec{R})$ term, states become unbounded if it is included in the potential. This δ function comes from the unnatural non-relativistic reduction and will become a smooth function with a finite range if this is calculated correctly. The standard way to include H_{SS} is to replace $\delta(\vec{R})$ by a smeared function

$$f(R) = (1/4\pi r_0^2)\exp(-R/r_0)/R, \quad \lim_{r_0\to\infty} f(R) = \delta(\vec{R}). \tag{2.4}$$

At very short distance, various relativistic effects, such as quark pair creation, arise and the original Coulomb-like behaviour will be distorted. The range of the smearing r_0 decreases as the quark mass increases. We use the following phenomenological formula for r_0:

$$r_0 = 0.08m^{-0.6}\ \text{fm}\ (m\ \text{in GeV}),$$

$$m = 2m_q m_{\bar{q}}/(m_q+m_{\bar{q}}). \tag{2.5}$$

We have checked that results we show here do not sensitively depend on the precise shape of the smearing function $f(r)$. We use the following potential parameters:

$$\alpha_s = 0.31, \quad R_1 = (4\alpha_s/3a)^{1/2},$$
$$a = 0.15\ \text{GeV}^{-2}, \quad b = 0.956\ \text{GeV}, \quad c = 2.05\ \text{GeV}^{-1},$$
$$d = aR_1 + 4\alpha_s/3R_1, \quad V_0 = -0.720\ \text{GeV}. \tag{2.6}$$

Quark masses used here are

$$m_u = m_d = 336\ \text{MeV}, \quad m_s = 575\ \text{MeV},$$
$$m_c = 1845\ \text{MeV}, \quad m_b = 5235\ \text{MeV}. \tag{2.7}$$

2.4. Experimental supports for the spin-spin force with a finite range

The energy levels predicted in this model (we call it model N) are shown in Table I. The agreement with the data is excellent. We can test if the range r_0 of H_{SS} is reasonable in the following way. For a P state multiplet, the centre of gravity (COG) of $^3P_3$, $^3P_1$, $^3P_0$

TABLE I

Magnetic dipole (M1) transition $1^- \to 0^- + \gamma$ or $0^- \to 1^- + \gamma$

Decay	μ_{PV}	Prediction		Experiment
		$I(k) = 1$ (keV)	$I(k)$ from model in Sec. 2 (keV)	
$\phi \to \eta\gamma$	$(\mu_u+\mu_d)\sin\phi_V \sin\phi_P + 2\mu_s \cos\phi_V \cos\phi_P$	78	62	63 ± 10
$\phi \to \pi\gamma$	$(-\mu_u+\mu_d)\sin\phi_V$	0	0	5.9 ± 2.3
$\rho^- \to \pi^-\gamma$	$\mu_u+\mu_d$	123	78	68 ± 10
$\rho^0 \to \eta\gamma$	$(-\mu_u+\mu_d)\sin\phi_P$	72	50	50 ± 13
$K^{*+} \to K^+\gamma$	$\mu_s+\mu_u$	142	109	60 ± 15
$K^{*0} \to K^0\gamma$	$\mu_s+\mu_p$	182	140	76 ± 37
$\omega \to \pi^0\gamma$	$(-\mu_u+\mu_d)\cos\phi_V$	1180	739	860 ± 76
$\omega \to \eta\gamma$	$(\mu_u+\mu_d)\sin\phi_P\cos\phi_V - 2\mu_s\cos\phi_P\sin\phi_V$	9.4	6.5	$3^{+2.5}_{-1.8}$
$\eta' \to \rho^0\gamma$	$(\mu_u-\mu_d)\cos\phi_P$	159	111	84 ± 34
$\eta' \to \omega\gamma$	$(\mu_u+\mu_d)\cos\phi_P\cos\phi_V + 2\mu_s\cos\phi_P\sin\phi_V$	14	10	8 ± 3

must coincide with $^1P_1$ if H_{SS} is a pointlike interaction, since the difference between them is proportional to $|\psi(0)|^2$ which is zero for the P state. From experimental values, one finds:

$$\text{COG of } (^3P_2, {}^3P_1, {}^3P_0) = \frac{1}{9}[5(^3P_2)+3(^3P_1)+(^3P_0)]$$
$$= \begin{cases} 1251\ \text{MeV} & \text{for} \quad A_2,\ A_1,\ \delta; \\ 1243\ \text{MeV} & \text{for} \quad f,\ D,\ S^*. \end{cases} \tag{2.8}$$

These COGs are higher than $^1P_1$ states.

$$\text{COG} \quad \text{of} \quad (A_2, A_1, \delta) - M(B) = 21 \text{ MeV},$$

$$\text{COG} \quad \text{of} \quad (f, D, S^*) - M(H) = 53 \text{ MeV}. \tag{2.9}$$

These are consistent with the prediction in our model

$$\text{COG} \quad \text{of} \quad (^3P_2, ^3P_1, ^3P_0) - M(^1P_1) = 31 \text{ MeV}. \tag{2.10}$$

This means the range of H_{SS} in our model is reasonable. It is very interesting to check our prediction for charmonium:

$$\text{COG} \quad \text{of} \quad (^3P_2, ^3P_1, ^3P_0) - M(^1P_1) = 10 \text{ MeV} \quad \text{for} \quad c\bar{c}. \tag{2.11}$$

In our model, the wave function of $^3S_1$ is substantially different from that of $^1S_0$. We can test our model in the following way. Leptonic and hadronic decay rates of J/ψ and η_c are given by:

$$\Gamma(J/\psi \to e^+e^- + \mu^+\mu^-) : \Gamma(J/\psi \to 3g) : \Gamma(\eta_c \to 2g)$$

$$= 2m_Q^{-2}e_Q^2\alpha|\psi_{^3S_1}(0)|^2 : \tfrac{10}{81}\alpha_s^3(\pi^2-9)\pi^{-1}m_Q^{-2}|\psi_{^3S_1}(0)| : \tfrac{2}{3}\alpha_s^2 m_Q^{-2}|\psi_{^1S_0}(0)|^2. \tag{2.12}$$

From these relations and from the experimental data $\Gamma_{\text{total}}(J/\psi) = 63 \pm 9$ keV and $\Gamma_{ee}(J/\psi) = 4.6 \pm 0.39$ keV, one gets $\alpha_s = 0.19$. Thus by using $\Gamma_{\text{total}}(\eta_c) = 12.4 \pm 4.1$ MeV, one finds the following ratio which agrees with our prediction:

$$|\psi_{^3S_1}(0)/\psi_{^1S_0}(0)|^2 = \tfrac{3}{2}\left(\frac{\alpha_s}{\alpha}\right)^2 \Gamma_{ee}(J/\psi)/\Gamma_{2g}(\eta_c)$$

$$= \begin{cases} 0.38 \pm 0.17 & \text{experiment;} \\ 0.271 & \text{theory.} \end{cases} \tag{2.13}$$

It should be noted that this ratio is one if H_{SS} is not included in the potential. If η_b is found, we can test our prediction $|\psi_{^3S_1}(0)/\psi_{^1S_0}(0)|^2 = 0.445$ (for $b\bar{b}$).

Other experimental evidence of the difference of the wave function between $^3S_1$ and $^1S_0$ states is given by the M1 transition rate [25]:

$$\Gamma_{if} = c\alpha\mu_{if}^2 k^3 |\langle f| \exp(i\vec{k}\cdot\vec{r}/2)\,|i\rangle|^2, \tag{2.14}$$

where $c = 4/3$ for $^3S_1 \to {}^1S_0 + \gamma$ and $c = 4$ for $^1S_0 \to {}^3S_1 + \gamma$. μ_{if} is listed in Table I. Since k is not large if $\psi_{^3S_1}(r) = \psi_{^1S_0}(r)$, we find $|\langle f| \exp(i\vec{k}\cdot\vec{r}/2)|i\rangle| = I(k) \approx 1$. However, ψ_i and ψ_f are not equal in our model; they do not overlap completely, thus $I(k) < 1$.

As shown in Table I, predicted values of decay rates for $I(k) = 1$ are too large, but those obtained in our model are smaller and much nearer to the data. This is the confirmation of Isgur's argument [26], although there might be other corrections to these decay rates.

TABLE II

Quarkonium spectra predicted by a potential model (Sec. 2)

$u\bar{u}$	1S	2S	3S
$^3S_1$	772 ρ(776)	1554 ρ′(1600)	2157
$^1S_0$	132 π(135)	1296 π′(1240)	1957

$u\bar{u}$	1P	2P	3P	1D	2D
$S=1$ $J=L+1$	1266 $\begin{cases} A_2(1318) \\ f(1273) \end{cases}$	1913 f*(1799)?	2466	1541	2144
$S=1$ $J=L$	1245 $\begin{cases} A_1(1230) \\ D(1285) \end{cases}$	1880	2422	1697	2253
$S=1$ $J=L-1$	1034 $\begin{cases} \delta(983) \\ S^*(975) \end{cases}$	1705 S*(1770)?	2257	1741	2272
$S=0$ $J=L$	1221 $\begin{cases} B(1230) \\ H(1190) \end{cases}$	1864	2413	1651	2204

$s\bar{s}$	1S	2S	3S
$^3S_1$	1010 φ(1020)	1713 φ′(1680)	2233
$^1S_0$	696	1568	2120

$s\bar{s}$	1P	2P	3P	1D
$S=1$ $J=L+1$	1496 f′(1515)	2047 $g_T(2160)$?	2512	1795
$S=1$ $J=L$	1428 $\underline{\underline{E}}$(1420)	1993	2460	1824
$S=1$ $J=L-1$	1278 $g_s(1240)$?	1877	2353	1807
$S=0$ $J=L$	1436	1999	2470	1808

$\bar{u}s$	1S	2S	3S
$^3S_1$	900 K*(892)	1648	2212
$^1S_0$	501 K(495)	1464	2069

TABLE II (continued)

$\bar{u}s$	1P	2P	1D
$S=1$ $J=L+1$	1399 K*(1434)	2002	1680
$S=1$ $J=L$	1383 Q_2(1410)	1978	1780
$S=1$ $J=L-1$	1196	1833	1801
$S=0$ $J=L$	1305 Q_1(1270)	1914	1738

	$\bar{u}c$	$\bar{s}c$	$\bar{u}b$
1^3S_1	2025 D*(2010)	1963 F(2018)	5359
1^1S_0	1891 D(1865)	2099 F*(2130)?	5310 B(5273)

	$c\bar{c}$	$b\bar{b}$
1^3S_1	3094 J/ψ(3097)	9462 Υ(9460)
1^1S_0	2979 η_c(2984)	9382
2^3S_1	3686 ψ(3685)	10031 Υ(10021)
2^1S_0	3627 η_c(3592)	10000
3^3S_1	4087 ψ(4030)	10379 Υ(10350)
4^3S_1	4412 ψ(4415)	10647 Υ(10566)
1^3P_2	3532 ψ(3551)	9928 Υ(9912)
1^3P_1	3488 ψ(3505)	9904 Υ(9892)
1^3P_0	3428 ψ(3414)	9873 Υ(9870)
1^1P_1	3496	9911

	$c\bar{c}$
1^3D_1	3772 ψ(3768)
2^3D_1	4141 ψ(4159)
	$b\bar{b}$
1^3D_1	10167
2^3D_1	10468
2^3P_2	10293 Υ(10264)
2^3P_1	10274 Υ(10249)
2^3P_0	10249 Υ(10231)
2^1P_1	10279

2.5. Fine structure of P state multiplets

Since potential parameters are adjusted to fit S wave $c\bar{c}$ and $b\bar{b}$ spectra and quark masses to fit S state masses, no parameters are left to fit P states. Nobody would be surprised if we had found completely wrong predictions for them. To our surprise, not only the COG but also the fine structure of P wave multiplets are in agreement with the data as shown in Table II. From this table, we notice a remarkable pattern of P wave multiplets of light quarkonium states. Three levels, $^3P_2$, $^3P_1$ and $^1P_1$ cluster and only $^3P_0$ becomes much lower and isolates. This pattern does not depend sensitively on the form of the potential [27]. Such clustering can be easily understood in the following way. By using Eq. (2.2) and the relation $\vec{S}_1 \cdot \vec{S}_2 = -3/4$ for $^1S_0$, $1/4$ for $^3S_1$, $\vec{L} \cdot \vec{S} = 1, -1, -2$ for $|\vec{L}+\vec{S}| = 2, 1, 0$,

one gets

$$M(^3P_2) = M_0 + A - \tfrac{2}{5}B + C,$$
$$M(^3P_1) = M_0 - A + 2B + C,$$
$$M(^3P_0) = M_0 - 2A - 4B + C,$$
$$M(^1P_1) = M_0 - 3C. \qquad (2.15)$$

From numerical calculations, one finds the relation $2B \gtrsim A \gtrsim B \gg C > 0$. C is small since the range of H_{SS} is small. We find this clustering for the following two extreme cases: (*i*) $A = 2B$, $C = 0$; $M(^3P_2) = M_0 + 8B/5$, $M(^3P_1) = M(^1P_1) = M_0$, $M(^3P_0) = M_0 - 8B$; (*ii*) $A = B$, $C = 0$; $M(^3P_1) = M_0 + B$, $M(^3P_2) = M_0 + 2B/3$, $M(^1P_1) = M_0$, $M(^3P_0) = M_0 - 6B$.

According to Jaffe [28], δ and S* are $q^2\bar{q}^2$ particles. One of the reasons for it is that they are much lower than other 1P multiplets. However, in our model, such isolation can naturally be understood by spin-dependent interactions. In the unitarized quarkonium model by Törnqvist [21], δ(980) and S*(985) are strongly shifted downward. It is desirable to include such effects in our model.

TABLE III

The ratio R_P in model N

	Theory	Experiment
$u\bar{u}+d\bar{d}$	0.06	0.14 ± 0.1
$u\bar{u}-d\bar{d}$	0.06	-0.03 ± 0.03
$s\bar{s}$	0.45	0.53?
$c\bar{c}$	0.73	0.48 ± 0.02
$b\bar{b}$ 1P	0.77	0.93 ± 0.1
$b\bar{b}$ 2P	0.76	0.85 ± 0.1

From Table II we compute the ratio $R_P = (M(^3P_2) - M(^3P_1)/(M(^3P_1) - M(^3P_0)) = (2A - 12B/5)/(A + 6B)$ and show the results in Table III. Scaling behaviours of the spin-dependent forces are

$$H_{LS}, H_T \sim m_Q^{-1}, H_{SS} \sim m_Q^{-3} \quad \text{for} \quad m_Q \lesssim 10\ \text{GeV},$$
$$H_{LS}, H_T \sim m_Q, H_{SS} \sim m_Q^{-5} \quad \text{for} \quad m_Q \gtrsim 100\ \text{GeV}. \qquad (2.16)$$

Thus the fine structure gets narrower as the quark mass increases up to around $m_Q \sim 50$ GeV and R_P approaches 0.8 [see Ref. [3]]. From Table II, we find such theoretical expectation is correct.

2.6. Q_1–Q_2 mixing

In Table II, $\bar{u}s$ P states are also listed. If we neglect $^3P_1 - {}^1P_1$ mixing [i.e., $D = 0$ in Eq. (2)], we find ($^3P_2$, $^3P_1$, $^3P_0$, $^1P_1$) = (1399, 1364, 1196, 1324 MeV). The term $D\vec{L} \cdot \vec{S}$

induces [29] the $^3P_1 - {}^1P_1$ mixing, which can be calculated by:

$$M(Q_1, Q_2) = \tfrac{1}{2}\,[M(^1P_1) + M(^3P_1) \pm \sqrt{\{M(^1P_1) - M(^3P_1)\}^2 + 8E^2}],$$

$$E = \tfrac{1}{4}\left(\frac{1}{m_1^2} - \frac{1}{m_2^2}\right)\int_0^\infty R_{1P}^2\left(\frac{dV_v}{dR} - \frac{dV_s}{dR}\right) RdR. \tag{2.17}$$

From numerical calculation, we find $E = 23.4$ MeV and $(^3P_2, Q_2, {}^3P_0, Q_1) = (1399, 1384, 1196, 1305\,\text{MeV})$ and mixing angle $= \text{Tan}^{-1}\sqrt{\{M(Q_2) - M(^3P_1)\}}/\sqrt{\{M(^3P_1) - M(Q_1)\}} = 30°$. Thus we find rough agreement with the data for $^3P_1$, Q_1, Q_2 but the prediction for $^3P_0$ is too low compared to $\kappa(1350)$, 0^+ meson.

We show similar calculations for the 2P state of $\bar{u}s$ in Table II. If we set $D = 0$ we obtain $(^3P_2', {}^3P_1', {}^3P_0', {}^1P_1') = (2002, 1966, 1833, 1926\,\text{MeV})$ and after the mixing we find $E = 17.1$ MeV, $(^3P_2', Q_2', {}^3P_0', Q_1') = (2002, 1978, 1833, 1914\,\text{MeV})$.

2.7. Inverted multiplet

As shown in Table I, D states of $u\bar{u} \pm d\bar{d}$, $\bar{u}s$ and $s\bar{s}$ are all inverted, i.e., the $^3D_3$ state is the lowest. The reason why D states are inverted (i.e., $A < 0$) while P states are not (i.e., $A > 0$) comes from the fact that V_v is of short range and V_s is of long range. From Eq. (2.2), one can see that for a wave function with small (large) rms radius, A is positive (negative). Experimentally, there are three D state candidates: $g(1690) = {}^3D_3$, $u\bar{u} - d\bar{d}$; $A_3(1680) = {}^1D_2$, $u\bar{u} - d\bar{d}$; $\omega(1670) = {}^3D_3$, $u\bar{u} + d\bar{d}$. This means that the D state multiplet is not yet inverted, thus it seems that our model does not work for D states any more. Schnitzer [29] argued that the P wave multiplet of $\bar{u}c$ states will be inverted. However, our model does not predict such an inverted multiplet for $\bar{u}c$.

2.8. Variational method and baryon spectrum [11]

We now try to compute the baryon spectrum by using the potential model shown above. We assume that the potential is described by the superposition of the two body forces. We use the standard variational method [30] to compute energy level. All the results shown below are computed by two Gaussian trial functions. If the number of trial functions is increased, we can get results with arbitral accuracy. If we increase the number of the Gaussian trial functions from two to three or four, the energy levels drop down at most one or two MeV. By using the Martin potential [4] we have numerically reproduced the result of the hyperspherical method by Richard [31].

We first try to compute the baryon spectrum by assuming $V_{qq}(R) = V_{q\bar{q}}(R)/2 = (V(\text{vector}) + V(\text{scalar}))/2$, where $V(\text{vector})$ and $V(\text{scalar})$ are taken from Eqs. (2.1) and (2.3). We find strong disagreement with the data, e.g., $(P, \Delta, \Omega^-) = (1.157, 1.320, 1.672\,\text{GeV})$ by using the quark masses given in Eq. (2.7). Next, we increase the vector part of the potential by 50%, although there is no theoretical justification, i.e., $V_{qq}(R) = (3\,V(\text{vector})/2 + V(\text{scalar}))/2$. We now find an agreement with the data for non-strange baryons, i.e.,

TABLE IV

Baryon resonance in model N

Resonance	Experiment (MeV)	Theory (MeV)
P	938	937
Δ	1232	1227
$(^2 8, 1^-)$ uuu	$\begin{cases} 1520 \pm 10 \\ 1540 \pm 20 \end{cases}$	1517
$(^4 8, 1^-)$ uuu	$\begin{cases} 1650 \pm 30 \\ 1675 \pm 15 \\ 1680 \pm 10 \end{cases}$	1638
$(^2 10, 1^-)$ uuu	$\begin{cases} 1625 \pm 25 \\ 1685 \pm 55 \end{cases}$	1614
Λ	1115.6	1102
Σ	1192	1207
Ω^-	1672	1663
Ξ	1320	1297
Ξ*	1530	1539
Σ*	1385	1389
Λ_c	2282	2262
Σ_c	2457	2468
Ξ_{cc}^* ucc		3594
Ξ_{cc} ucc		3738
Ω_c css		2758

Δ, P, $(^2 10, 1^-)$, $(^2 8, 1^-)$, $(^4 8, 1^-)$ by again assuming $m_u = 336$ MeV, where our notation is $(^{2S+1}\mathrm{SU}(3), L^P)$. For all strange baryons, we find too small masses if we take the non--strange quark mass $m_s = 575$ MeV determined to fit meson spectra.

We assume that the masses which we are using here are effective ones. Thus, it is not necessary that the quark mass in a meson must be the same as that in a baryon. In the following, we choose a larger quark mass, $m_s = 660$ MeV and $m_c = 1970$ MeV, than those for mesons. The results are shown in Table IV. The agreement with the data is excellent. As for $L = 1$ qqq state (q = u or d), we include only H_{SS}. H_{LS} and H_T are neglected. The mixing between two octet states is also neglected. The rough agreement of our results with the data shows that H_{LS} and T_T and the mixing effect are not very important. If H_{SS} is a pointlike interaction, the $(^4 8, 1^-)$ state and the $(^2 10, 1^-)$ state are degenerate, but if not, $(^4 8, 1^-)$ is higher than $(^2 10, 1^-)$ [see Ref. [32]]. In our model, $(^4 8, 1^-)$ is higher than $(^2 10, 1^-)$ by 24 MeV, but the experimental situation is not clear.

3. *OZI allowed decays of quarkonium states*

3.1. The quark pair creation model (QPC)

A. Le Yaouanc et al. [14] have proposed the quark pair creation model in order to describe the OZI allowed decay (Fig. 1). If a low energy light quark pair is created, many gluons will be exchanged in this process, and the single gluon exchange diagram is unlikely to dominate since α_s is large. In such a case, initial $q\bar{q}$'s will stay as

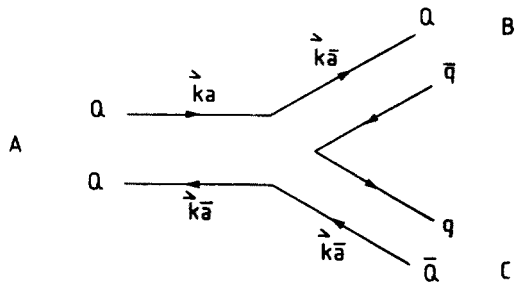

Fig. 1. Schematical representation of a decay $A \to B + C$ according to QPC

spectators. This means the created quark pair must have the same quantum number as the vacuum, i.e., 0^{++}, thus the created pair must be a $^3P_0$ state. The spatial dependence of the overlap integral is given by the following matrix element:

$$I^{L_A}_{m_P,m_A} = \gamma_{QPC} \int d\vec{q}\, y_1^{m_P}(2\vec{q} + h_Q\vec{k})\psi_A^{m_A}(\vec{q} - \tfrac{1}{2}h_q\vec{k})\psi_B^*(\vec{q})\psi_C^*(\vec{q}),$$

$$h_q = \frac{2m_Q}{m_q + m_Q}, \qquad h_Q = \frac{2m_q}{m_q + m_Q}, \tag{3.1}$$

where k is the absolute value of B and C's momenta in A's centre of mass system, γ_{QPC} is a coupling constant describing the strength of the pair creation and other notation is clear from Fig. 1. The reduced matrix elements are defined for the two allowed angular momenta between final mesons; $L = L_A \pm 1$.

$$\mathscr{L}_{L_A}(\mp) = \sum_{m_A m_B} I^{L_A}_{m_A,m_B}(L_A, m_A, 1, m_P | L_A \mp 1, 0)\sqrt{\frac{4\pi}{2(L_A \mp 1)+1}}. \tag{3.2}$$

The amplitude for a given partial wave is given by:

$$M = \sum_{S_T, L = L_A \pm 1} \begin{bmatrix} i_Q & i_q & I_B \\ i_Q & i_q & I_C \\ I_A & 0 & I_A \end{bmatrix} \begin{bmatrix} S_Q & S_q & S_B \\ S_Q & S_q & S_C \\ S_A & 1 & S_T \end{bmatrix} \begin{bmatrix} L_A & S_A & J_A \\ 1 & 1 & 0 \\ L & S_T & J_A \end{bmatrix} \varepsilon \mathscr{L}_{L_A}(\pm). \tag{3.3}$$

The decay width is given by:

$$\Gamma = 2\pi |M|^2 \frac{E_B E_C}{M_A} k. \tag{3.4}$$

By using the harmonic oscillator model, Ader et al. [15] calculated decay widths of various mesons (light quarkonium as well as charmonium), and found that $\gamma_{QPC} \sim 3.4$ for all mesons.

In order to compute the overlap integral, we must use a special potential model. We use the following potential model [model II in Ref. [33]], which is obtained from Eq. (2.1) by replacing $V_1(R)$ by the following function:

$$V_1(R) = V_{AF} + aR,$$

$$V_{AF}(R) = -\tfrac{4}{3}\frac{\alpha_s(R)}{R}, \quad \alpha_s(R) = \frac{12\pi}{25}\cdot\frac{1}{\ln(\mu/R)}, \tag{3.5}$$

$$\mu = (\Lambda e^{\gamma})^{-1}, \quad \Lambda = 0.5\ \text{GeV}, \quad \gamma = 0.5772,$$

where $V_{AF}(R) = -8/25 \exp(1)/\mu$ for $R \geqslant \mu \exp(-1)$. Results which we are going to show do not depend on the precise shape of the potential. As a typical example, we show the reduced matrix $\mathscr{L}_{\psi(3S)\to D\bar{D}}(k)$ defined by Eq. (3.2) as a function of the decay momentum in Fig. 2. For small k, one can assume $\Gamma \propto k^{2l+1}$, which corresponds to $\mathscr{L}(k) \propto k$. This approximation is good for $k \lesssim 100$ MeV in this case. Decay momenta for $\psi(3S) \to D\bar{D}$,

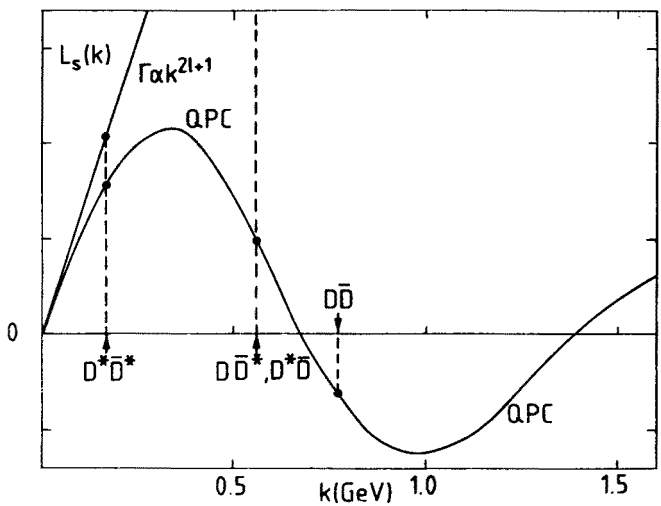

Fig. 2. Reduced matrix for $\psi(3S) \to D\bar{D}$, $D\bar{D}^* + D^*\bar{D}$, $D^*\bar{D}^*$ predicted by the QPC is compared to the assumption $\mathscr{L} \propto k$, i.e., $\Gamma \propto k^{2l+1}$

$D\bar{D}^*$, $D^*\bar{D}^*$ are plotted by arrows in Fig. 2. One can see from this figure that the QPC predicts [13, 19] a much smaller decay width for $\psi(3S) \to D\bar{D}$ than the assumption $\Gamma \propto k^{2l+1}$, due to the node structure (by a factor ~ 100). Such suppression is indeed observed and the QPC is supported. The QPC also explains the small branching ratio for $\Gamma(\varrho' \to \pi\pi)$ which is due to a similar reason.

3.2. OZI allowed decay of $\Upsilon(4S)$ and the QPC

$\Upsilon(4S)$ is the first resonance above threshold. From the invariant mass of the decay product of $B^{\pm,0}$, the mass of the B meson (average of $B^{\pm}$ and B^0) is determined experimentally. Thus, we now know [8]

$$\Delta \equiv M(\Upsilon''') - 2M(B) = 32.4 \pm 3.0 \pm 4.0 \text{ MeV}. \tag{3.6}$$

In Fig. 3 we plot the decay rate predicted by the QPC, where γ_{QPC} is fixed [19] by the decay rate of $c\bar{c}$ above threshold. The model which we are using now is identical to the Bigi and Ono model [34]. In Fig. 3 we also plot decay width obtained by simple phase space $\Gamma \propto k^{2l+1}$. Other decay modes $\Upsilon(4S) \to B\bar{B}^*$, $B^*\bar{B}$, $B^*\bar{B}^*$ will be forbidden since we expect $B^* - B \sim 45$ MeV [33].

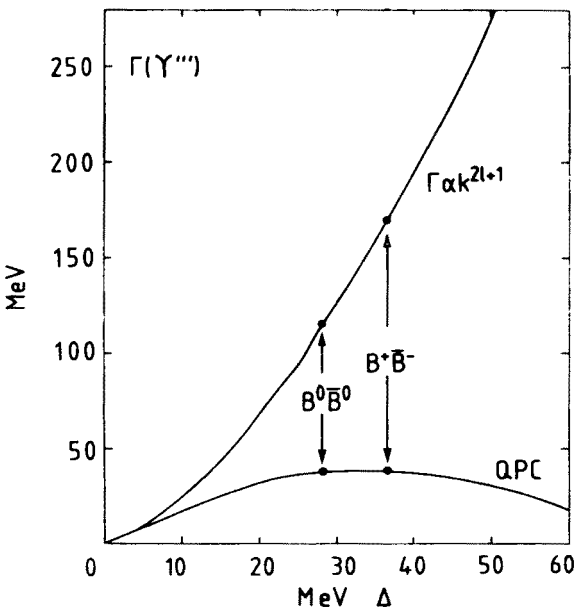

Fig. 3. Decay width of Υ''' as a function of $\Delta = M(\Upsilon''') - 2M(B)$ predicted by the QPC is compared to the assumption $\Gamma \propto k^{2l+1}$

From this graph we find that we are around the top of the peak of the QPC curve and the approximation $\Gamma \propto k^{2l+1}$ breaks down completely in this region. The approximation $\Gamma \propto k^{2l+1}$ is good only for $k \lesssim 5$ MeV. By assuming $B^0 \pm B^{\pm} = 4.4$ MeV and $\Gamma \propto k^{2l+1}$, the CESR group has found $B(\Upsilon(4S) \to B^+B^-) = 0.60 \pm 0.02$, $B(\Upsilon(4S) \to B^0\bar{B}^0) = 0.40 \pm 0.02$. However, if we use the curve predicted by the QPC we find $B(\Upsilon(4S) \to B^+B^-) = B(\Upsilon(4S) \to B^0\bar{B}^0) = 0.5$. Thus we must say that $\Gamma \propto k^{2l+1}$ *cannot be used in this region.*

One might think that the QPC predicts too large a decay width for $\Upsilon(4S)$ compared to the data $\Gamma_{\text{total}} \sim 14$ MeV. However, since the decay rate changes very rapidly as a function of Δ, the shape of the resonance is very distorted from the simple Breit-Wigner shape.

Actual resonance shape is expressed by [34]

$$\Delta R(w) \propto \frac{\Gamma(w)}{(w_0-w)^2+\Gamma(w)^2/4}\,. \tag{3.7}$$

If w increases starting from w_0, the $\Gamma(w)^2/4$ term in the denominator increases very rapidly due to $\Gamma(\Upsilon(4S) \to B^*\bar{B}+B\bar{B}^*)$, thus the upper tail of the resonance is cut off. For the lower tail of the resonance, the $(w_0-w)^2$ term dominates and the actual resonance width becomes smaller than $\Gamma(w)$ at the peak.

By using recent CESR data on the resonance shape of Υ''', we have computed the χ^2 value for various Δ. We find that χ^2 does not change very much between $\Delta = 10$ and 40 MeV. Thus, we conclude that if the resonance width is determined by a Gaussian fit, the obtained width does not necessarily correspond to $\Gamma(w)$ at the peak in the QPC.

4. Quarkonium states and glueball states

4.1. Is $g_T(2160)$ a glueball state? [35]

Recently a peak was found [36] in $\pi^-P \to Xn \to \phi\phi n$ by the BNL/CCNY group:

$$g_T(2160),\ \text{mass} = 2160\pm 37\ \text{MeV}, \quad \Gamma = 315\pm 62\ \text{MeV}, \quad J^{PC} = 2^{++}. \tag{4.1}$$

According to Lindenbaum [37], this is a glueball candidate because this process is doubly OZI forbidden and must be strongly suppressed if $g_T(2160)$ is a quarkonium state. However, we can show that this process is not suppressed if $g_T(2160)$ is a 2^3P_2, 2^{++}, $s\bar{s}$ state.

We first study the decay rate of g_T by using the QPC. Results [35] are

$$\Gamma(\phi\phi) = 97\ \text{MeV}, \quad \Gamma(K^*\bar{K}^*) = 387\ \text{MeV}, \quad \Gamma(K\bar{K}) = 35\ \text{MeV},$$

$$\Gamma(\eta\eta) = 1.6\ \text{MeV}, \quad \Gamma(K\bar{K}^*+K^*\bar{K}) = 1.7\ \text{MeV}. \tag{4.2}$$

As seen from this, g_T couples very strongly to $K^*\bar{K}^*$ and $\phi\phi$. This is understandable since these two are only S wave decays while others are D wave decays. Thus, the following production scheme must be enhanced strongly:

$$\pi^-p \to K^*\bar{K}^*n \xrightarrow[\text{(S-wave)}]{} g_Tn \xrightarrow[\text{(S-wave)}]{} \phi\phi n. \tag{A}$$

According to Lindenbaum, the process (*A*) should be suppressed by the OZI rule (he called it the "quark line rule"). He refers to the following process

$$\pi^-p \to K^+K^-n \to \phi n, \tag{B}$$

where the suppression factor is ~ 100. However, there are the following reasons why the process (*A*) is much more enhanced than the process (*B*):

(*i*) The process (*B*) needs three-gluon exchange [37] due to the spin of ϕ. On the other hand, only two-gluon exchange is sufficient for g_T production, since g_T has $J^{PC} = 2^{++}$.

(*ii*) The S wave transition $K^*\bar{K}^* \to g_T$ is much easier than the P wave transition $K\bar{K} \to \phi$.

Since these transitions are near the threshold, the centrifugal barrier greatly suppresses the latter transition.

(*iii*) $\sigma(\pi p \to K^*\bar{K}^* n)$ is much larger than $\sigma(\pi p \to K\bar{K} n)$ due to spin factor.

The mass of $g_T(= 2160 \pm 37$ MeV) is slightly larger than the potential model expectation (~ 2050 MeV, see Table I) if g_T is $s\bar{s}$. However, the mass of this resonance is determined from the $\phi\phi$ peak, which is only 120 MeV above the $\phi\phi$ threshold while the width is 315 MeV. If the mass of this resonance is determined by the $K^*\bar{K}^*$ peak, the value might be different. Related work on $g_T(2160)$ was also done by Minami [38].

4.2. Is $\theta(1640)$ a glueball state? [35]

The Crystal Ball group found [39] a resonance in the process $J/\psi \to \gamma\theta(1640)$

$$\begin{aligned}
&\Gamma(\theta \to \text{all}) = 200 \pm 100 \text{ MeV}, \quad M(\theta) = 1640 \pm 50 \text{ MeV}, \\
&BR(J/\psi \to \theta\gamma)BR(\theta \to \eta\eta) = (0.38 \pm 0.16) \times 10^{-3}, \\
&BR(J/\psi \to \theta\gamma)BR(\theta \to K\bar{K}) = (1.24 \pm 0.18 \pm 0.5) \times 10^{-3}, \\
&BR(J/\psi \to \theta\gamma)BR(\theta \to \varrho\varrho) = (3.75 \pm 1.05 \pm 1.2) \times 10^{-3}, \\
&BR(J/\psi \to \theta\gamma)BR(\theta \to \pi\pi) < 2.4 \times 10^{-4} (90\% \text{ C.L.}).
\end{aligned} \tag{4.3}$$

In the following, we consider [35] the various assignments for θ and check if such assignments are reasonable.

(*i*) $\theta = 2P$, $(u\bar{u}+d\bar{d})/\sqrt{2}$.

In this assumption we find $M(\theta) = 1913$ MeV (see Table I), which is much higher than the experimental value 1640 MeV. There is experimental evidence [40, 41] for the 2^{++} meson $f^*(1799)$ which is much nearer to our expectation, thus a better candidate for 2P, $(u\bar{u}+d\bar{d})/\sqrt{2}$. However, this resonance needs further experimental confirmation [42]. The branching ratio can be computed by using the QPC if $\theta = 2P$, $(u\bar{u}+d\bar{d})/\sqrt{2}$:

$$\begin{aligned}
&BR(\theta \to \varrho\varrho) : BR(\theta \to K\bar{K}) : BR(\theta \to \eta\eta) : BR(\theta \to \pi\pi) \\
&= \begin{cases} 1 & : 0.0019 : 0.0009 : 0.23 \quad \text{theory;} \\ 1 & : 0.33 : 0.1 : < 0.06 \quad \text{experiment.} \end{cases}
\end{aligned} \tag{4.4}$$

Thus, this is an unlikely possibility.

(*ii*) $\theta =$ *glueball*

Assuming SU(3) invariant decay and the phase space $\tilde{\Gamma} \propto k^{2l+1}$, one obtains [35]

$$\Gamma(\theta \to \eta\eta) : \Gamma(\theta \to K\bar{K}) : \Gamma(\theta \to \pi\pi) = \begin{cases} 1 : 5.7 : 12.3 & \text{theory;} \\ 1 : 3.3 : < 0.63 & \text{experiment.} \end{cases} \tag{4.5}$$

Instead of looking for other models which predict SU(3) breaking or more complicated phase space, we consider the following possibility.

(*iii*) $\theta =$ *mixture of* 1P, $(u\bar{u}+d\bar{d})/\sqrt{2}$ *and a glueball*

We again use the QPC for the qq part. If one assumes a pointlike glueball, i.e., $\Gamma \propto k^5$ for glueball decay, one finds [35] $\Gamma(\theta \to K\bar{K}) = 4.35$ MeV and $\Gamma(\theta \to \eta\eta) = 0.76$ MeV,

which are too small. On the other hand, if one assumes a glueball state with finite size, one gets a reasonable branching ratio [35] for $\theta \to \eta\eta$, $K\bar{K}$, $\pi\pi$, $\varrho\varrho$. In this case, 10% of θ is 1P, $(u\bar{u}+d\bar{d})/\sqrt{2}$ and 90% of θ is the glueball.

(iv) θ = *mixture of* 2P, $(u\bar{u}+d\bar{d})/\sqrt{2}$ *and a glueball*

In this case, the QPC predicts too small a total decay width for θ ($\Gamma \lesssim 77$ MeV) compared to the experimental value.

Thus our conclusion from the decay properties of θ is that the 1P, $(u\bar{u}+d\bar{d})/\sqrt{2}$ + glueball interpretation is the most promising one. It might be necessary to consider mixing together 1P, 2P and a glueball and, if necessary, $s\bar{s}$ states. However, we do not have enough data to fix so many mixing parameters.

5. Toponium states

5.1. Above threshold [43]

The number of S states below threshold increases as the quark mass increases. A typical potential model predicts [43] seven S states below threshold for $m_Q = 20$ GeV. According to the QPC, the decay width of the resonance above threshold becomes large as m_Q increases. Several charmonium states above threshold have been observed and their decay widths range from 20 to 50 MeV. Only one bottomium state $\Upsilon(4S)$ which is very near to the threshold has been observed, and other states above threshold are probably too broad to see. Toponium states above threshold will be even broader and probably impossible to find experimentally unless they are very near the threshold or node of an important channel [43].

5.2. Below threshold

Branching ratios of toponium states (1S, 2S, 3S, 1P, 2P, 1D) are calculated in Ref. [20]. Since the ground state energy level falls deep into the potential for heavy toponium states, the behaviour of the potential near origin ($R \lesssim 0.1$ fm) becomes important for low-lying states. For example, we can use potentials which, for short distances, approach the asymptotic behaviour predicted by a perturbative two-loop calculation [44]. Several attempts have been made to connect this potential to the large distance region [5, 20, 44]. We show one of them [20]

$$V(R) = -\frac{16\pi}{25}\cdot\frac{1}{R\ln f(\Lambda_{\overline{\mathrm{MS}}}R)}$$

$$\times\left[1+\frac{2\gamma_E+\frac{53}{75}}{\ln f(\Lambda_{\overline{\mathrm{MS}}}R)}-\frac{462\ln\ln f(\Lambda_{\overline{\mathrm{MS}}}R)}{625\ln f(\Lambda_{\overline{\mathrm{MS}}}R)}\right]+a\sqrt{R}+c, \tag{5.1}$$

$$f(\Lambda_{\overline{\mathrm{MS}}}R) = 1/(\Lambda_{\overline{\mathrm{MS}}}R)^2+b,$$

$$\Lambda_{\overline{\mathrm{MS}}} = 140\ \mathrm{MeV}, \quad a = 0.63\ \mathrm{GeV}^{3/2}, \quad b = 20, \quad c = -1.39\ \mathrm{GeV}$$

$$m_c = 1.9\ \mathrm{GeV}, \quad m_b = 5.255\ \mathrm{GeV}.$$

As a less singular (at the origin) choice, this potential is used and as a singular choice, the Richardson potential [45] is used to study the branching ratio of toponium states. The conclusions which we found are the following. For all quarkonium states the branching ratio of weak decays increases rapidly and becomes important (or dominant) for $m_t \gtrsim 35$ GeV. Unlike charmonium and bottomium cases, toponium P states will be quite narrow and their radiative decays will dominate for $m_t \lesssim 35$ GeV. The branching ratio $nS \to n'S+\gamma$ is reasonably large in this region. Detection of P states in radiative cascade decays will be extremely difficult for $m_t \gtrsim 35$ GeV, since weak decays become important and they deplete production of P states and radiative $P \to S\gamma$ decays at the same time.

6. Unitarized quarkonium model (UQM) for $c\bar{c}$ and $b\bar{b}$ states [22]

6.1. UQM

Because of unitarity, the naive potential model such as models shown until now is only an approximation, even within a non-relativistic framework. The $D\bar{D}$, etc., channels couple strongly to charmonium, giving large widths above threshold. Because of analyticity they contribute mass shifts to charmonium states. The full mass matrix is a sum of a bare term M^2_{bare} and a hadronic mass renormalization term $\Pi(s)$:

$$M^2_{n,m}(s) = M^2_{\text{bare},n,m} + \Pi_{n,m}(s), \quad n, m = 1S, 2S, 1D, \ldots . \tag{6.1}$$

Im $\Pi(s)$ is given by a sum over the threshold:

$$\text{Im}\, \Pi^{A}_{n,m}(s) = \sum_{BC = D\bar{D}, F\bar{F}, \ldots} \text{Im}\, \Pi^{ABC}_{n,m}(s), \tag{6.2}$$

$$\text{Im}\, \Pi^{ABC}_{n,m}(s) = -V^{BC}_{A,n}(s) V^{BC}_{A,m}(s) k^B 2\pi E^B E^C \theta(s-(m_B+m_C)^2), \tag{6.3}$$

where $V^{BC}_{A,n}(s)$ is the vertex function which is calculated by Eq. (3.3) ($V = M$). Since our vertex functions make Im Π vanish exponentially for large s, one has automatically a cut-off in our model; Re $\Pi(s)$ can be computed from an unsubtracted dispersion relation

$$\text{Re}\, \Pi_{nm}(s) = -\frac{1}{\pi} \int \text{Im}\, \Pi_{nm}(s')/(s-s')ds' . \tag{6.4}$$

The diagonal elements of Re $\Pi(s)$ are in general negative and contribute a negative mass shift to the resonance. Equations (6.1)–(6.3) define the mass matrix in the reference frame of the bare states. The physical states are obtained after diagonalization;

$$M^2_{\text{diag}}(s) = \alpha^{-1}(s) M^2(s) \alpha(s), \tag{6.5}$$

where the mixing matrix α satisfies $\alpha^T\alpha = 1$, i.e., α is an orthogonal matrix since M^2 is symmetric. Neglecting the contribution, our normalization ($s = m_R^2$) is:

$$\sum_n |\alpha^T_{nm}(s = m_R^2)|^2 = 1. \tag{6.6}$$

To estimate the OZI allowed coupling we use the QPC which is already described in Section 3 in detail. If one were to neglect the mixing induced by α in Eq. (6.5), the total width would simply be given by Eq. (3.4) (M in Section 3 is V here). In the unitarized model, the widths are obtained after diagonalization of M^2 in Eq. (6.1). Then

$$\Gamma_A^{\text{total}} = -\text{Im}\, M_{\text{diag}}^2(s)/\sqrt{s}\,|_{s=m_A} \tag{6.7}$$

and the physical resonance mass

$$M_A = M_{\text{diag}}^2(s)/\sqrt{s}\,|_{s=m_A^2}. \tag{6.8}$$

The pair creation parameter γ_{QPC} in Eq. (3.1) is the only free parameter which is essentially determined by the best-known experimental width. It is known that γ_{QPC} is fairly flavour-independent [15], thus we use the same $\gamma_{\text{QPC}} = 3.029$ for $c\bar{c}$ and $b\bar{b}$ states.

We show in Fig. 4 the mass shifts for $c\bar{c}$ and $b\bar{b}$ states which are all negative. First of all, we notice relatively large mass shifts of the states just above threshold, i.e., $\psi(1D)$ and $\Upsilon(4S)$. It is known [46] that the experimental mass values of such states are higher than the prediction by typical potential models. Therefore, we nicely confirm that $\psi(1D)$ and $\Upsilon(4S)$ are affected by the threshold effects.

For $c\bar{c}$ the higher radial excitations have relatively small shifts because of the node structure of the wave functions. On the other hand, thresholds for $b\bar{b}$ are much higher

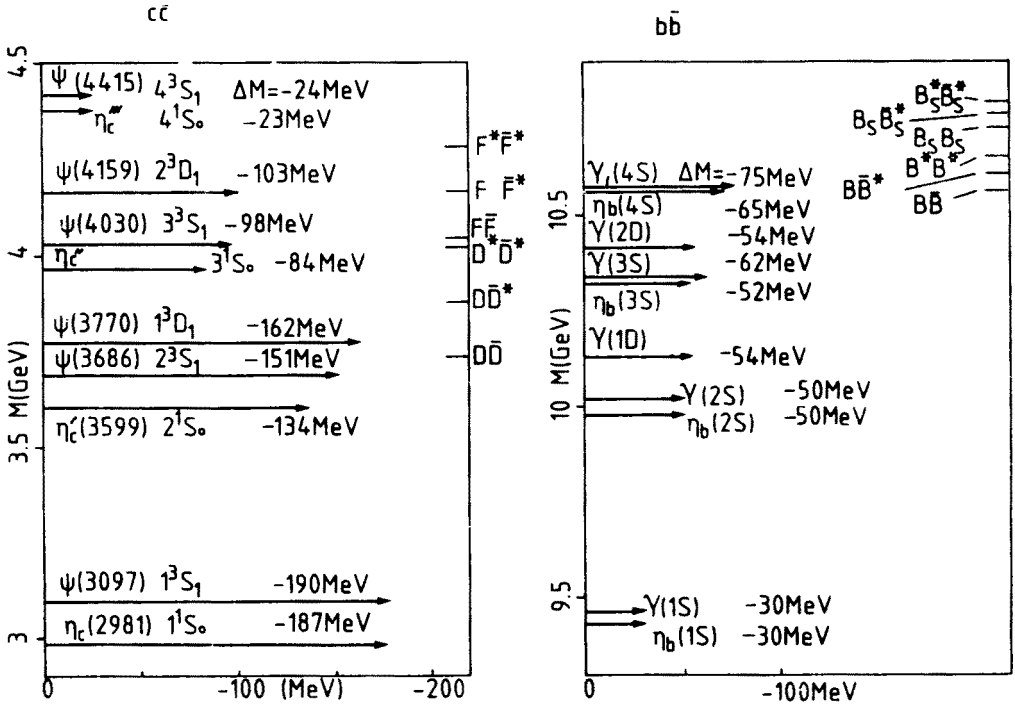

Fig. 4. Mass shifts due to unitarity effects. Positions of thresholds are shown

than for $c\bar{c}$ (see Fig. 4), thus lower $b\bar{b}$ states have small mass shifts; i.e., thresholds are too far from lower $b\bar{b}$ states. In addition to this, the thresholds for $b\bar{b}$, i.e., $B\bar{B}$, $B\bar{B}^*$, $B_s\bar{B}_s$, etc., are more densely located than those for $c\bar{c}$, i.e., $D\bar{D}$, $D\bar{D}^*$, $F\bar{F}$, etc. Thus higher excited Υ states, such as $\Upsilon(3S)$ and $\Upsilon(4S)$ have relatively large shifts due to this group of thresholds and overcome the reduction due to node structure.

6.2. Mass shifts for J/ψ and η_c

The mass shift for n^3S_1 is not much different from that for n^1S_0. Experimentally known hyperfine splittings are

$$\Delta M = M(J/\psi) - M(\eta_c) = 116 \pm 4 \text{ MeV} \quad [47],$$

$$\Delta M^* = M(\psi') - M(\eta_c') = 93 \pm 5 \text{ MeV} \quad [47, 48],$$

$$\text{i.e., } \Delta M^*/\Delta M = 0.8. \tag{6.9}$$

Unfolding unitarity effects, we get hyperfine splittings for the bare mass

$$\Delta M(\text{bare}) = \Delta M + 3 \text{ MeV} = 119 \text{ MeV},$$

$$\Delta M^*(\text{bare}) = \Delta M^* + 17 \text{ MeV} = 110 \text{ MeV}. \tag{6.10}$$

Thus we find $\Delta M^*(\text{bare})/\Delta M(\text{bare}) = 0.92$, which is difficult to accommodate by a potential model whose typical prediction is $\Delta M^*/\Delta M \sim 0.5$. Similar results were found by Martin and Richard [49] by using a different model.

6.3. Mass shifts for P state multiplets [50]

In Section 2.5, we have shown that the fine structure of the P state multiplet can be roughly reproduced only by the Breit-Fermi Hamiltonian. Unitarity effects do not badly destroy already successful predictions of the potential model. For example, all four P states $^3P_{2,1,0}$, $^1P_1$ will be shifted with the same amount if D* has the same mass as D and all four P states degenerate. Mass shifts for ($^3P_2$, $^3P_1$, $^3P_0$, $^1P_1$) states are [50]

$$\begin{aligned}
&(-186, -180, -170, -182 \text{ MeV}) \quad \text{for} \quad 1P, c\bar{c};\\
&(\ -45, \ -44, \ -43, \ -44 \text{ MeV}) \quad \text{for} \quad 1P, b\bar{b};\\
&(\ -58, \ -56, \ -55, \ -57 \text{ MeV}) \quad \text{for} \quad 2P, b\bar{b},
\end{aligned} \tag{6.11}$$

where $^3P_2 - {}^3F_2$ mixing is taken into account.

This means the mass shifts have almost no effect on the fine structure for $b\bar{b}$ states while for $c\bar{c}$, if we unfold the unitarity effects, the splitting $^3P_2 - {}^3P_0$ becomes smaller.

6.4. Mass shifts for radially excited states and the potentials for bare spectra

As seen in Fig. 4, mass shifts for $b\bar{b}$ systems are completely different from those for $c\bar{c}$ systems. Since mass shifts for $b\bar{b}$ states are not very large, any potential which reasonably fits the physical $b\bar{b}$ spectrum can also fit bare mass spectra, if the constant term in the

potential is modified. As for $c\bar{c}$ systems, mass shifts are larger and we have to change potential shape. We have found that the potential which fits the bare mass spectra (we call it the *bare potential*) has a lower slope for $r > 1$ fm than the potential which fits the physical spectra. This means that the bare potential rises slower than the linear one, since the change of potential for large r does not affect the $b\bar{b}$ spectra appreciably because the rms radius of wave functions for $b\bar{b}$ states is small.

We now show three examples of bare potentials.

(*a*) Martin potential [4]:

$$V(R) = -7.873 + 6.8698\, R^{0.1}, \quad R \text{ in GeV}, \quad m_c = 1.8 \text{ GeV}, \quad m_b = 5.1 \text{ GeV}; \tag{6.12}$$

(*b*) $R^{2/3}$ + Coulomb potential:

$$V(R) = -\tfrac{4}{3}\frac{\alpha_s}{R} + BR^{2/3} - A,$$

$$A = 0.98 \text{ GeV}, \quad B = 0.35, \quad \alpha_s = 0.35, \quad m_c = 1.9 \text{ GeV}, \quad m_b = 5.215 \text{ GeV}; \tag{6.13}$$

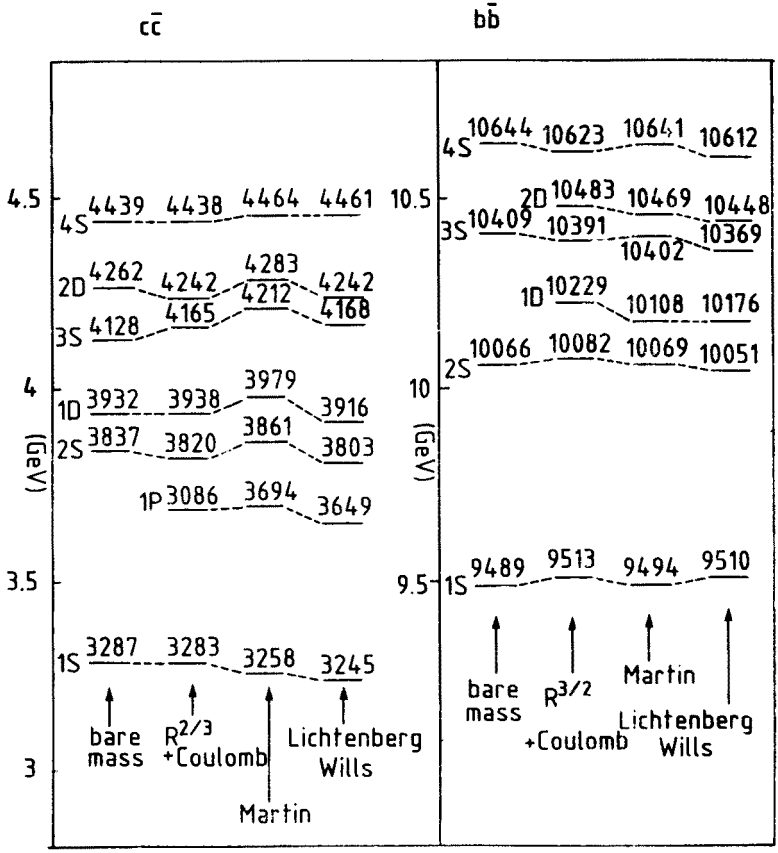

Fig. 5. The bare mass spectrum which is obtained by unfolding unitarity effects is compared with the ones computed by three potentials

(*c*) Lichtenberg-Wills potential [6]:

$$V(R) = \frac{8\pi}{25} \cdot \frac{(1-\lambda R)^2}{R \ln \lambda R} + A; \tag{6.14}$$

$$\lambda = \Lambda e^{\gamma}, \quad \gamma = 0.5772, \quad \Lambda = 350 \text{ MeV},$$

$$A = -850 \text{ MeV}, \quad m_c = 1.9 \text{ GeV}, \quad m_b = 5.21 \text{ GeV}.$$

We have changed the potential parameters and quark masses from original papers for (*a*) and (*c*). Lichtenberg and Wills used $\Lambda = 676$ MeV, but after unfolding unitarity effects, we find $\Lambda = 350$ MeV. Experimentally, $\Lambda_{\overline{\text{MS}}} = 50-400$ MeV. The above three potentials are almost numerically identical between 0.1 fm and 1.5 fm, although their short-distance behaviour ($r < 0.1$ fm) is quite different. In Fig. 5, we compare the bare mass spectrum with predictions by these three potentials. Agreement with the data is quite satisfactory.

6.5. S–D mixing and e^+e^- decay rates

By using the mixing matrix $\alpha(s)$ obtained in Eq. (6.5), one can calculate the e^+e^- decay rate of quarkonia, which is given by

$$\Gamma(Q\bar{Q} \to e^+e^-) = \frac{4\alpha^2 e_Q^2}{M(Q\bar{Q})^2} \left| \sum_{k=\text{S-states}} \alpha_{ik}^{\mathrm{T}} \psi_k^{(0)}(0) + \frac{5}{2\sqrt{2}\, m_Q^2} \sum_{k=\text{D-states}} \alpha_{ik}^{\mathrm{T}} \psi_k^{(0)\prime\prime}(0) \right|^2 \tag{6.15}$$

with obvious notation. The wave functions $\psi_k^{(0)}$ must be determined by using a bare potential. Results are compared with the data in Table V. We also list results obtained by neglecting unitarity effects. (We choose as typical potentials (*i*) Coulomb + linear [51]; (*ii*) Buchmüller-Tye potential [5].) As seen from this Table, if the unitarity effect is unfolded, we find remarkable improvements for Γ_{ee} decay rates, especially for $c\bar{c}$. $\Gamma_{ee}(3S)/\Gamma_{ee}(1S)$ and $\Gamma_{ee}(4S)/\Gamma_{ee}(1S)$ decrease and $\Gamma_{ee}(1D)/\Gamma_{ee}(1S)$ increases.

The increase of $\Gamma_{ee}(1D)$ and $\Gamma_{ee}(2D)$ is due to the S–D mixing, and the decrease of $\Gamma_{ee}(3S)$ and $\Gamma_{ee}(4S)$ is due partly to the S–D mixing and partly to the potential behaviour for large R (since these potentials increase slower than the linear rising one, the wave functions for higher excited states spread out). We do not find any way to accommodate the extraordinarily large branching ratio:

$$\Gamma_{ee}(2D) = 770 \pm 230 \text{ eV} \tag{6.16}$$

although our prediction is much nearer to the experimental value than that of potential models. A similar conclusion is drawn by the Cornell model [51].

TABLE V

Theoretical predictions of decay rates $\Gamma_{ee} = \Gamma(Q\bar{Q} \to e\bar{e})$ for cases when (*i*) unitarity effects are unfolded, (*ii*) unitary effects are neglected, are compared with the data

		Unitarity effects unfolded			Not unfolded	
$c\bar{c}$	Data (Ref. [52])	$R^{2/3}$ + Coulomb	Martin	Lichtenberg Wills	Coulomb + linear (Ref. [51])	Buchmüller–Tye (Ref. [5])
$\Gamma_{ee}(2S)/\Gamma_{ee}(1S)$	0.45 ± 0.08	0.351	0.348	0.373	0.44	0.46
$\Gamma_{ee}(3S)/\Gamma_{ee}(1S)$	0.16 ± 0.04	0.247	0.227	0.269	0.31	0.32
$\Gamma_{ee}(4S)/\Gamma_{ee}(1S)$	0.11 ± 0.04	0.154	0.133	0.171	0.23	0.25
$\Gamma_{ee}(1D)/\Gamma_{ee}(1S)$	0.056 ± 0.011	0.031	0.039	0.036	~ 0	~ 0
$\Gamma_{ee}(2D)/\Gamma_{ee}(1S)$	0.17 ± 0.06	0.011	0.013	0.013	~ 0	~ 0
$b\bar{b}$						
$\Gamma_{ee}(2S)/\Gamma_{ee}(1S)$	0.46 ± 0.03	0.378	0.534	0.464	0.36	0.44
$\Gamma_{ee}(3S)/\Gamma_{ee}(1S)$	0.33 ± 0.03	0.293	0.429	0.379	0.25	0.32
$\Gamma_{ee}(4S)/\Gamma_{ee}(1S)$	0.23 ± 0.02	0.240	0.355	0.325	0.20	0.26
$\Gamma_{ee}(1D)/\Gamma_{ee}(1S)$	—	0.00027	0.00014	0.00025	~ 0	~ 0
$\Gamma_{ee}(2D)/\Gamma_{ee}(1S)$	< 0.04	0.0010	0.00081	0.0011	~ 0	~ 0
$\Gamma_{ee}(3D)/\Gamma_{ee}(1S)$	—	0.0127	0.0210	0.0183	~ 0	~ 0

There exist related works, e.g., the Cornell model [51], the Nijmegen model [53] and some others [54, 55]. We believe that our model has various advantages:

(*i*) We use the QPC which is already confirmed to be able to explain various decay processes.

(*ii*) We are consistently using a QCD motivated potential. The Cornell group used a Coulomb plus linear potential for the $c\bar{c}$ part and a harmonic oscillator potential for D and D* mesons.

(*iii*) Cornell's model calculation breaks down completely for higher excited $c\bar{c}$ states (e.g., 4S states), as was admitted by themselves. They found $M(4^3S_1) = 4625$ MeV, which is as much as 210 MeV higher than the experimental value 4415 MeV. Another problem is that they found $2^3D_1 - 3^3S_1 = 5$ MeV, while the experimental value is 129 ± 25 MeV. We have found much better agreement with the data including 4S and 2D − 3S.

REFERENCES

[1] J. J. Aubert et al., *Phys. Rev. Lett.* **33**, 1404 (1974); J. E. Augustin et al., *Phys. Rev. Lett.* **33**, 1406 (1974); G. S. Abrams et al., *Phys. Rev. Lett.* **33**, 1453 (1974).

[2] E. Eichten et al., *Phys. Rev. Lett.* **34**, 369 (1975).

[3] H. Krasemann, S. Ono, *Nucl. Phys.* **B154**, 283 (1979).

[4] A. Martin, *Phys. Lett.* **100B**, 511 (1981).

[5] W. Buchmüller, H. H. Tye, *Phys. Rev.* **D24**, 132 (1981).

[6] D. B. Lichtenberg, J. G. Wills, *Nuovo Cimento* **47**, 483 (1978); G. Fogleman et al., *Lett. Nuovo Cimento* **26**, 369 (1979).

[7] S. Ono, *Lett. Nuovo Cimento* **8**, 378 (1973); *Phys. Rev.* **D9**, 2005 (1974); *Phys. Rev.* **D9**, 2670 (1974).
[8] J. Lee-Franzini, Talk at 7th International Conference on Meson Spectroscopy, BNL, Upton, April 1983.
[9] N. Isgur, G. Karl, *Phys. Rev.* **D18**, 4187 (1978).
[10] D. Gromes, Talk given at the IVth International Conference on Baryon Resonance, Toronto, July 1980.
[11] S. Ono, F. Schöberl, *Phys. Lett.* **118B**, 419 (1982).
[12] M. B. Gavela et al., *Phys. Lett.* **79B**, 459 (1978).
[13] A. Le Yaouanc et al., *Phys. Lett.* **71B**, 397 (1977); **72B**, 57 (1977).
[14] A. Le Yaouanc et al., *Phys. Rev.* **D8**, 2228 (1973).
[15] J. P. Ader, B. Bonnier, S. Sood, Bordeaux Univ. Preprint PTB-116 (1980).
[16] W. B. Kaufmann, R. J. Jacob, *Phys. Rev.* **D10**, 1051 (1974); M. Böhm, H. Joos, M. Krammer, *Nucl. Phys.* **B69**, 349 (1974).
[17] E. Eichten et al., *Phys. Rev.* **D17**, 3090 (1978).
[18] I. I. Bigi, S. Ono, *Nucl. Phys.* **B189**, 229 (1981).
[19] S. Ono, *Phys. Rev.* **D23**, 1118 (1981).
[20] H. Kühn, S. Ono, *Z. Phys.* **C21**, 395 (1984).
[21] N. A. Törnqvist, *Ann. Phys.* (USA) **123**, 1 (1979); M. Roos, N. A. Törnqvist, *Z. Phys.* **C5**, 205 (1980); N. A. Törnqvist, *Phys. Rev. Lett.* **49**, 624 (1982); *Nucl. Phys.* **B203**, 268 (1982).
[22] K. Heikkilä, S. Ono, N. A. Törnqvist, Proc. of XVIIIth Rencontre de Moriond, Jan. 1983; Helsinki Univ. preprint HU-TFT-83-4, *Phys. Rev.* **D29**, 110 (1984).
[23] M. Frank, P. J. O'Donnell, Toronto Univ. preprint, March 1983.
[24] P. Falkensteiner, D. Flamm, F. Schöberl, *Phys. Lett.* **B**, to be published.
[25] S. Ono, *Phys. Rev.* **D27**, 1203 (1983).
[26] N. Isgur, *Phys. Rev. Lett.* **36**, 1262 (1976).
[27] S. Ono, *Phys. Rev.* **D28**, 558, (1983).
[28] R. J. Jaffe, Talk at the International Symposium on Lepton and Photon Interaction at High Energies, Bonn, August 1981.
[29] H. J. Schnitzer, *Phys. Rev.* **D18**, 3482 (1978).
[30] D. Flamm, F. Schöberl, *Introduction to the Quark Model of Elementary Particles*, Vol. I, Gordon & Breach, New York 1982.
[31] J. M. Richard, *Phys. Lett.* **100B**, 515 (1981).
[32] D. Gromes, Talk given at IVth International Conference on Baryon Resonance, Toronto, July 1980.
[33] S. Ono, *Phys. Rev.* **D20**, 2975 (1979).
[34] I. I. Bigi, S. Ono, in Ref. [18].
[35] S. Ono, O. Pene, *Z. Phys.* **C21**, 109 (1983).
[36] A. Etkin et al., *Phys. Rev. Lett.* **49**, 1620 (1982).
[37] S. L. Lindenbaum, Proc. of XVIth Rencontre de Moriond, Elementary Particle Physics Meetings, Les Arcs, Savoie, March 1981.
[38] S. Minami, Osaka City Univ. preprint OCU-98 (1982); OCU-102 (1803).
[39] E. D. Bloom, XXI Int. Conf. on High Energy Physics, Paris (July 1982).
[40] N. Cason, contributed to 7th Int. Conf. on Meson Spectroscopy, BNL, Apr. 1983.
[41] L. Montanet, talk at 7th Int. Conf. on Meson Spectroscopy, BNL, Apr. 1983.
[42] L. Montanet, private communication.
[43] S. Ono, *Z. Phys.* **C8**, 7 (1981).
[44] K. Igi, K. Hikasa, Univ. of Tokyo preprint UT-399 (1982); O. Abe et al., *Phys. Rev.* **D27**, 675 (1983); J. Morishita et al., Kobe-82-08.
[45] J. I. Richardson, *Phys. Lett.* **82B**, 272 (1979).
[46] K. Berkelman, Proc. of the 20th Int. Conf. on High Energy Physics, Madison, Wisconsin, July 1980.
[47] C. Edward et al., *Phys. Rev. Lett.* **48**, 70 (1982).

[48] D. L. Scharre, Proceedings of 1981 International Symposium on Lepton and Photon Interaction at High Energies, Bonn, August 1981.
[49] A. Martin, J.-M. Richard, *Phys. Lett.* **115B**, 323 (1982).
[50] S. Ono, N. A. Törnqvist, CERN preprint Ref. TH3729, *Z. Phys.* C, to be published.
[51] E. Eichten et al., *Phys. Rev.* **D21**, 203 (1980).
[52] Particle data group, M. Roos et al., *Phys. Lett.* **111B**, 1 (1982).
[53] E. van Beveren, C. Dullemond, G. Rupp, *Phys. Rev.* **D21**, 772 (1980); E. van Beveren, Nijmegen preprint THEF-NYM-82.8, to be published in *Z. Phys.* C; THEF-NYM-83.04, to be published in *Z. Phys.* C.
[54] S. Jacobs, K. J. Miller, M. G. Olsson, *Phys. Rev. Lett.* **18**, 1181 (1983).
[55] H. G. Dosch, MIT preprint CTP # 959 (1981).